Acta Crystallographica Section D
Biological Crystallography
ISSN 0907-4449

Low-density crystal packing of human protein kinase CK2 catalytic subunit in complex with resorufin or other ligands: a tool to study the unique hinge-region plasticity of the enzyme without packing bias

Karsten Klopffleisch,[a] Olaf-Georg Issinger[b] and Karsten Niefind[a]*

[a]Department für Chemie, Institut für Biochemie, Universität zu Köln, Otto-Fischer-Strasse 12–14, D-50674 Köln, Germany, and [b]Institut for Biokemi og Molekylaer Biologi, Syddansk Universitet, Campusvej 55, DK-5230 Odense, Denmark

Correspondence e-mail: karsten.niefind@uni-koeln.de

Received 18 December 2011
Accepted 16 April 2012

PDB References:
CK2α^{1-335}–resorufin, 3u9c; CK2α^{1-325}/CK2$\alpha'^{327-350}$–AMPPN(P), 3u87.

A low-resolution structure of the catalytic subunit CK2α of human protein kinase CK2 (formerly known as casein kinase 2) in complex with the ATP-competitive inhibitor resorufin is presented. The structure supplements previous human CK2α structures in which the interdomain hinge/helix αD region adopts a closed conformation correlating to a canonically established catalytic spine as is typical for eukaryotic protein kinases. In the corresponding crystal packing the hinge/helix αD region is nearly unaffected by crystal contacts, so that largely unbiased conformational adaptions are possible. This is documented by published human CK2α structures with the same crystal packing but with an open hinge/helix αD region, one of which has been redetermined here with a higher symmetry. An overview of all published human CK2α crystal packings serves as the basis for a discussion of the factors that determine whether the open or the closed hinge/helix αD conformation is adopted. Lyotropic salts in crystallization support the closed conformation, in which the Phe121 side chain complements the hydrophobic catalytic spine ensemble. Consequently, genuine ligand effects on the hinge/helix αD conformation can be best studied under moderate salt conditions. Ligands that stabilize either the open or the closed conformation by hydrogen bonds are known, but a general rule is not yet apparent.

1. Introduction

1.1. The hinge/αD region of eukaryotic protein kinases

The catalytic core of eukaryotic protein kinases (EPKs), which were structurally characterized for the first time in the case of cAMP-dependent protein kinase (CAPK; Knighton *et al.*, 1991), is composed of two domains that harbour the ATP-binding site between them (Fig. 1). Catalytically competent ATP binding is accomplished by determinants of the two domains themselves and additionally by the hinge region (Zheng *et al.*, 1993), which links them in a way that permits limited interdomain mobility (Cox *et al.*, 1994).

The hinge forms hydrogen bonds to the adenine moiety of ATP *via* its peptide backbone (Zheng *et al.*, 1993; Fig. 2*a*). Moreover, in CAPK and many other EPKs it possesses a ribose anchor, *i.e.* a negatively charged side chain that co-ordinates the 2′- and 3′-hydroxy groups of the ATP ribose and is typically located in the transition section between the hinge and the subsequent helix αD (Fig. 1). Consequently, this extended hinge region (termed the 'hinge/αD region' in the following) is also a pharmacologically important determinant for the binding of ATP-competitive EPK inhibitors (Traxler & Furet, 1999).

In recent years, Taylor and coworkers (Kornev *et al.*, 2008; Taylor & Kornev, 2011) have developed the spine concept, which assigns additional significance to the hinge/αD region: in CAPK, Met128, which is the starting residue of helix αD, is an integral part of the so-called 'catalytic spine'. The catalytic spine and its pendant, the regulatory spine, are two conserved stacks of hydrophobic residues that penetrate the catalytic core and cross the interdomain space (Fig. 1). The regulatory spine is a *sine qua non* of an active EPK, while the catalytic spine requires the adenine group of ATP for full completion (Fig. 1); it is thus periodically opened and re-established during the catalytic cycle.

1.2. Hinge/αD-region plasticity in human CK2α

The study presented here deals with the hinge/αD region of CK2α, the catalytic subunit of protein kinase CK2, which

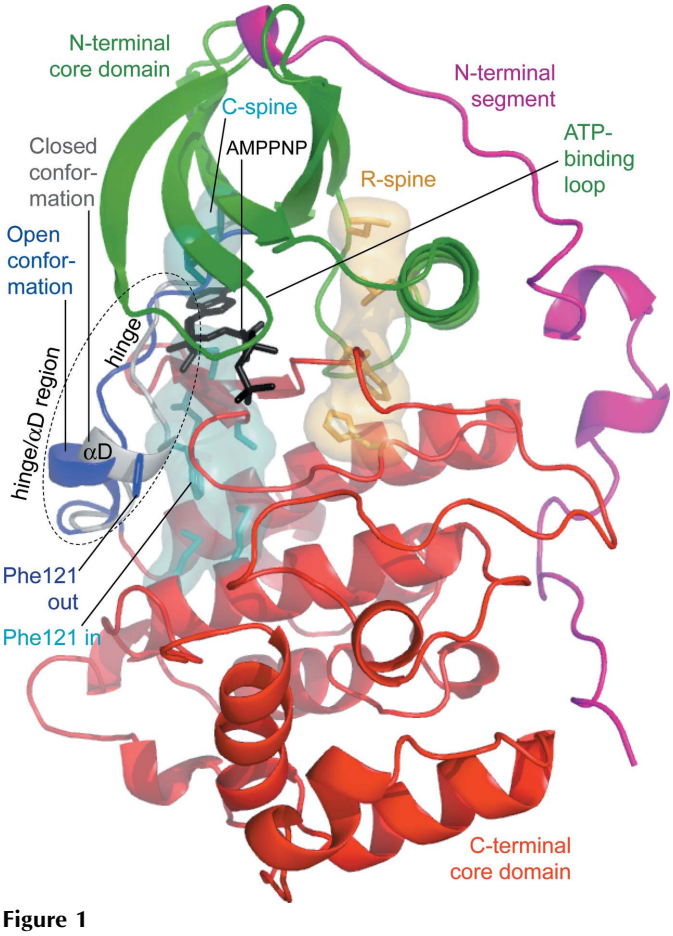

Figure 1
Overview of protein kinase architecture using the example of CK2α. The catalytic protein kinase core, indicated in green (N-terminal domain) or red (C-terminal domain), is penetrated by the regulatory spine (R-spine) and the catalytic spine (C-spine). The hinge/αD region is drawn in blue (open conformation with Phe121 turned towards the outside) or grey (closed conformation with Phe121 turned towards the inside, *i.e.* as part of the C-spine). The N-terminal segment (magenta) folding back towards the C-terminal domain is a typical feature of CK2α. This figure was prepared using *PyMOL* (Schrödinger LLC) from the CK2α^{1-325}/CK2$\alpha'^{327-350}$–AMPPN(P) complex structure (PDB entry 3u87). The closed conformation of the hinge/helix αD region (coloured grey) was drawn from the CK2α^{1-335}–resorufin complex (PDB entry 3u9c).

can associate with the noncatalytic subunit CK2β to form a heterotetrameric holoenzyme (Niefind *et al.*, 2001). CK2 is an acidophilic Ser/Thr kinase of the CMGC subgroup of EPKs. Its association with a variety of diseases (Guerra & Issinger, 2008) renders it an attractive drug target (Trembley *et al.*, 2010). CK2 is therefore the subject of inhibitor-design studies (Battistutta, 2009), and in this context the fluorescent dye resorufin (Fig. 3*a*) has recently been identified as an ATP-competitive CK2 inhibitor (Sandholt *et al.*, 2009; Fritz *et al.*, 2009).

In the first structure of the CK2α subunit to be determined (Niefind *et al.*, 1998), an unconventional hinge/αD region conformation (compared with CAPK and the other EPK structures known at the time) was discovered. This EPK-atypical conformation was found in all subsequent CK2α and CK2 holoenzyme structures determined until 2005, when the first CK2α structure with a conformation of the hinge/αD region more similar to that in CAPK was published (Yde *et al.*, 2005).

This alternative hinge/αD conformation, which was referred to as the 'closed' conformation (grey region in Fig. 1) by Raaf, Brunstein *et al.* (2008) in order to distinguish it from the 'open' conformation (blue region in Fig. 1) originally described (Niefind *et al.*, 1998), occurred in several further CK2α structures (Raaf, Klopffleisch *et al.*, 2008; Zhou *et al.*, 2009; Raaf *et al.*, 2009; López-Ramos *et al.*, 2010). An initial cluster analysis (Raaf, Klopffleisch *et al.*, 2008) suggested that maize CK2α occurs exclusively with the open hinge/αD conformation while human CK2α can adopt either conformation, a distinction that was confirmed by a rigorous statistical analysis including all CK2α structures available at the time (Niefind *et al.*, 2009). A survey of the Protein Data Bank (PDB) revealed that nine of the 28 entries containing human CK2α (which were without exception C-terminal deletion constructs or degradation products) showed the hinge/αD region in its closed version (shown in bold in Table 1).

The functional and pharmacological importance of the hinge/αD region makes it desirable to understand the factors that govern its conformational state in order to finally be capable of predicting it. A necessary prerequisite to approach this goal is to estimate and to eliminate the effects of crystal-packing constraints and of special crystallization conditions. Currently, the majority of the human CK2α structures in the PDB originate from a monoclinic crystal form (No. 1 in Table 1) in which the packing density is fairly high (39% solvent content). Both hinge/αD conformations can exist in these crystals, but the open conformation is distinctly more frequent (>80%) and occurs in particular in the apo structure PDB entry 1na7, *i.e.* in the absence of a stabilizing ATP-site ligand (Pechkova *et al.*, 2003). These observations indicate a preference for the open conformation in this crystal form, possibly owing to the fact that in the open conformation crystalline neighbours cover 254 Å^2 of the surface area of the hinge/αD region on average, which is significantly more than in the closed conformation (157.2 Å^2; Table 1).

To avoid any crystal-packing bias, here we compare a set of human CK2α structures, among them a novel CK2α–resorufin

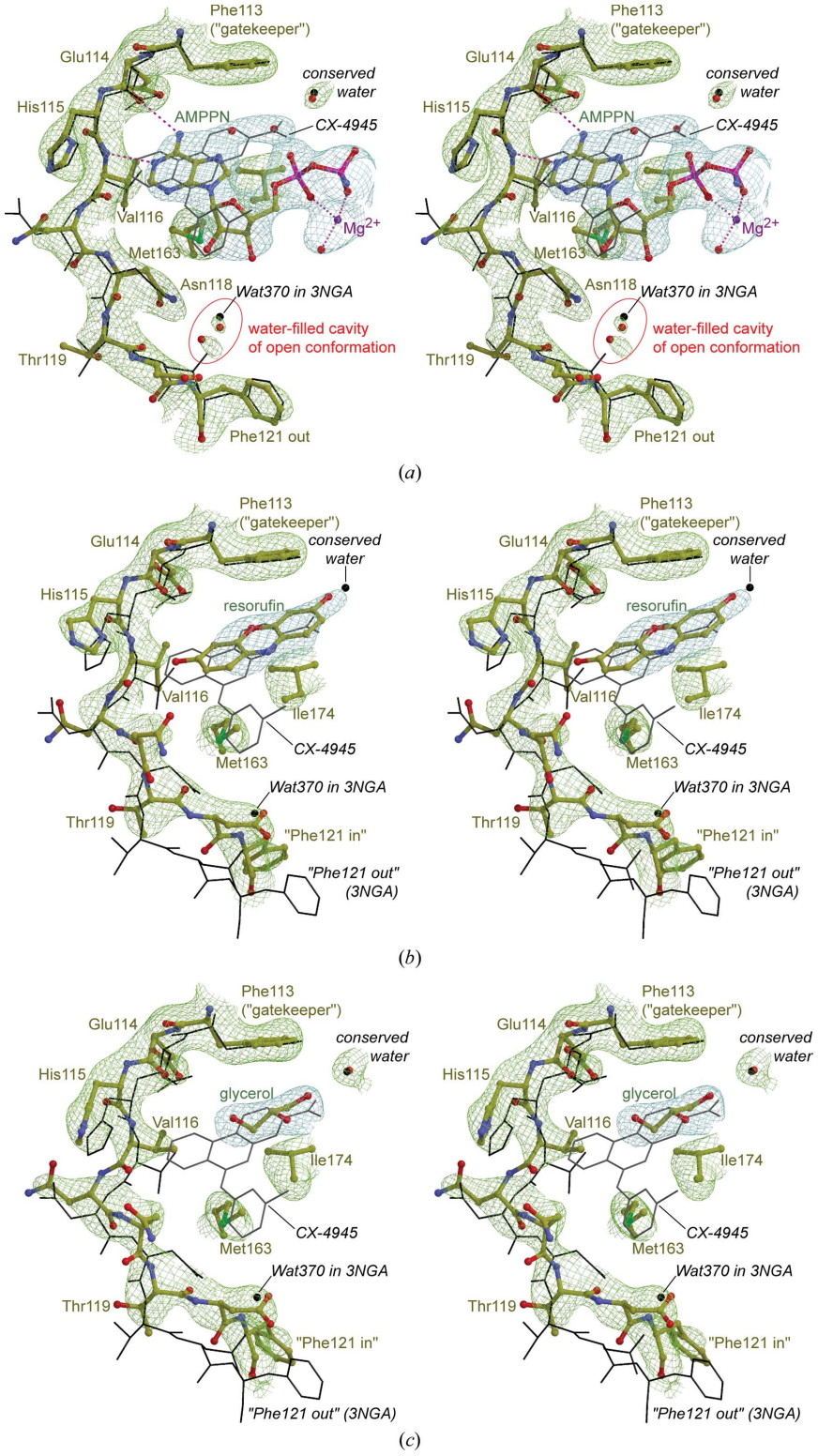

Figure 2
The hinge/αD-region conformations in the four structures with low-density tetragonal crystal packing. In all parts of the figure, which was prepared with a combination of *BobScript* (Esnouf, 1997) and *Raster3D* (Merritt & Bacon, 1997), the structure of the complex of CK2α with the inhibitor CX-4945 (PDB entry 3nga; Ferguson *et al.*, 2011) serves as a reference representing the open hinge/αD conformation (black bonds, black water molecules, grey CX-4945 molecule). The pieces of electron density stem from maps that were averaged over the two CK2α chains of the asymmetric unit using the corresponding routines in *Coot* (Emsley *et al.*, 2010). A cutoff level of 1σ was applied for the illustration. Colour code for pieces of averaged density: ATP-site ligand, blue; enzyme matrix, green. (*a*) CK2α^{1-325}/CK2$\alpha'^{327-350}$ in complex with AMPPN(P) and magnesium ions. Two hydrogen bonds from AMPPN to the hinge region as well as coordinative bonds to the Mg^{2+} ion are drawn as magenta dotted lines. (*b*) CK2α^{1-335} in complex with resorufin. (*c*) Rat CK2α^{1-335} (identical to human CK2α^{1-335}) crystallized without a defined ATP-site ligand. Glycerol from the cryosolution instead occupies the ATP site.

Table 1
Overview of human CK2α crystal packing in the PDB.

Fields that refer exclusively to the closed hinge/helix αD conformation are shown in bold.

No.	Space group, unit-cell parameters (Å, °)	Mean solvent content (%)	Hinge/helix αD conformation	PDB codes with ligands occupying the ATP site†	Mean surface of hinge/αD region covered by crystal contacts‡ (Å^2)	Crystallization essentials		
						Main precipitants§	Salt additives¶	Method of enzyme/ligand combination
1	$P2_1$, a = 59, b = 46, c = 63, β = 112	39.0	**Closed**	**3bqc, 3c13 (emodin); 3mb6 (a difurandicarboxylic acid derivative)**	**157.2**	**30–32% PEG 4000 (3bqc, 3c13); 36% PEG MME 5000 (3mb6)**	**$(NH_4)_2SO_4$ (3mb6); Li_2SO_4 (3bqc); $CH_3COO(NH_4)$ (3c13)**	**Pre-incubation (3bqc, 3c13); soaking (3mb6)**
			Open	1na7 (apo); 1pjk, 2pvr [(adenylyl imidodiphosphate (AMPPNP)]; 3mb7 (a difurandicarboxylic acid derivative); 3owj, 3owk, 3owl (3-pyridocarbazole derivatives); 3pe1, 3pe2, 3r0t (CX-4945 and relatives)	254.0	25% PEG 3500 (1na7); 30–32% PEG 4000 (3pe1, 3pe2, 3r0t); 36% PEG MME 5000 (1pjk, 2pvr, 3mb6, 3owj, 3owk, 3owl)	$(NH_4)_2SO_4$ (3mb7, 3owj, 3owk, 3owl); Li_2SO_4 (3pe1, 3pe2, 3r0t); CH_3COONa (1na7)	Pre-incubation (3pe1, 3pe2, 3rot); cocrystallization (1pjk, 2pvr); soaking (3mb7, 3owj, 3owk, 3owl)
2	$P2_12_12_1$, a = 48, b = 76, c = 78	31.0	Open	2zjw (ellagic acid); 3amy (apigenin); 3at2 (ethylene glycol); 3at3, 3at4 (pyridine derivatives)	154.7	25% ethylene glycol		Pre-incubation
3	$P2_12_12_1$, a = 49, b = 62, c = 117	45.1	Open	3nsz [adenylyl phosphoramidate (AMPPN)]	17.5	26% PEG 4000	$(NH_4)_2SO_4$	Cocrystallization
4a	***P*4$_3$, *a* = *b* = 72, *c* = 126**	**38.7**	**Closed**	**3fwq (apo); 3h30 (5,6-dichloro-ribofuranosyl benzimidazole); 3juh [adenylyl imidodiphosphate (AMPPNP)]**	**6.3**	**2 *M* $(NH_4)_2SO_4$, 2 *M* NaCl (3fwq); 2.2 *M* sodium citrate (3h30); 1.5 *M* $(NH_4)_2SO_4$, 0.2 *M* sodium citrate (3juh)**		**Pre-incubation (3h30); cocrystallization (3juh)**
4b	***P*4$_3$, *a* = *b* = 72, *c* = 133**	**42.9**		**3rps (a tetrabromobenzotriazole derivative)**	**3.2**	**4 *M* NaCl, 0.1 *M* sodium citrate**		**Pre-incubation**
5	$P4_32_12$, a = b = 127, c = 125	61.6	**Closed**	**2r7i (apo); 3u9c (resorufin)**	**22.1**	**25% PEG 3350 (2r7i); 30% PEG 8000 (3u9c)**	**Li_2SO_4 (2r7i); $(NH_4)_2SO_4$ (3u9c)**	**Pre-incubation (3u9c)**
			Open	3nga (CX-4945); 3u87 (formerly 3rp0; chain *A*, AMPPNP; chain *B*, AMPPN)	37.9	26% PEG 4000 (3nga); 15% PEG 8000, 15% glycerol (3u87)	$(NH_4)_2SO_4$	Soaking (3nga); cocrystallization (3u87)
6	$P6_3$, a = b = 175, c = 93	61.7	Open	1jwh (CK2 holoenzyme; chain *A*, AMPPNP, chain *B*, apo)	Chain *A*, 74.4; chain *B*, 256.7	20% PEG 3350	K_2HPO_4	Cocrystallization

† For literature references and chemical details, see the corresponding entries in the PDB (http://www.rcsb.org). ‡ Calculated using *AREAIMOL* from the *CCP*4 suite (Winn *et al.*, 2011). All nonprotein atoms were neglected in these calculations. § Abbreviations: PEG, polyethylene glycol; PEG MME, polyethylene glycol monomethylether. ¶ Further ions were introduced by buffer substances and by sodium chloride in the protein stock solution.

structure, originating from tetragonal crystals grown under similar conditions to the monoclinic crystals but comprising a crystalline arrangement in which the hinge/αD region is largely free from crystal contacts.

2. Materials and methods

2.1. Selection of human CK2α structures

The CK2α structures primarily discussed here were determined from tetragonal crystals (space group $P4_32_12$, packing No. 5 in Table 1) containing two independent chains per asymmetric subunit. The loose packing of these crystals (mean solvent content of 61.6%) results in diffraction data sets with poor resolution (Table 2) but also results in sufficient space to allow plasticity of the hinge/αD region.

To date, this low-density tetragonal crystal form has appeared three times in the literature representing different functional states, namely (i) with apo CK2α from rat (fragment 1–335, which is identical to human CK2α^{1-335}; PDB entry 2r7i; Zhou *et al.*, 2009); (ii) with human CK2α^{1-335} in complex with the high-affinity ATP-competitive inhibitor CX-4945 (Siddiqui-Jain *et al.*, 2010; PDB entry 3nga; Ferguson *et al.*, 2011); and (iii) with the chimeric construct CK2α^{1-325}/CK2$\alpha'^{327-350}$ in complex with the ATP analogue AMPPNP (PDB entry 3rp0; Bischoff, Raaf *et al.*, 2011). Here, we optimized two of these structures as far as possible (see below) and supplemented them with the cocrystal structure of human CK2α^{1-335} with resorufin (Table 2).

It is notable that the crystallization conditions were similar in all four cases, with a medium-length polyethylene glycol as a precipitant, a slightly acidic pH value (5.5–6.5) and a significant concentration of sulfate ions (0.17–0.20 *M*). The CK2α^{1-335}–CX-4945 complex structure (PDB entry 3nga) is a special case insofar as it did not result from cocrystallization; rather, the crystals were originally grown in the presence of AMPPNP, which was subsequently substituted by extensive soaking (Ferguson *et al.*, 2011). However, a recent high-

Table 2
Data-collection and refinement statistics.

Values in parentheses are for the highest shell.

Structure	CK2α^{1-335}–resorufin (PDB entry 3u9c)	CK2α^{1-325}/CK2$\alpha'^{327-350}$–AMPPN(P) (PDB entry 3u87; formerly 3rp0)	Apo CK2α^{1-335} (PDB entry 2r7i)
X-ray diffraction data collection			
Space group	$P4_32_12$	$P4_32_12$	$P4_32_12$
Unit-cell parameters (Å)	$a = b = 127.78$, $c = 125.77$	$a = b = 127.82$, $c = 125.33$	$a = b = 127.52$, $c = 126.41$
Resolution (Å)	19.9–3.2 (3.37–3.20)	36.7–2.9 (3.06–2.90)	50.0–3.0 (3.13–3.00)†
R_{merge} (%)	17.8 (68.9)	10.3 (69.5)	15.4 (64.8)†
$\langle I/\sigma(I)\rangle$	14.6 (3.9)	17.5 (3.6)	14.2 (2.8)†
Completeness (%)	99.6 (100.0)	99.5 (99.8)	99.6 (100.0)†
Multiplicity	10.2 (10.4)	9.7 (10.0)	7.2 (6.8)†
Wilson B factor (Å^2)	70.6	78.3	42.0†
Structure refinement and validation			
Resolution (Å)	19.9–3.2	36.7–2.9	20.0–3.0
No. of reflections	17632	23394	20291
No. of reflections in test set	881	1202	1050
R_{work}/R_{free} (%)	20.1/23.1	18.6/21.8	20.8/24.8
Composition of asymmetric unit			
Protomers	2	2	2
Missing (disordered) residues	Met1, Arg333–Gly335	Met1, Gln331–Arg349	Met1, Arg333–Gly335
ATP-site ligands	2 resorufin	1 AMPPNP, 1 AMPPN	—
Further ligands	7 SO_4^{2-}, 1 Cl^-, 5 glycerol	4 Mg^{2+}, 2 Cl^-, 2 SO_4^{2-}, 2 glycerol	9 SO_4^{2-}, 7 glycerol
Water molecules	55	51	61
Ramachandran plot quality‡			
Most favoured	547 [90.7%]	535 [89.8%]	535 [89.0%]
Additionally allowed	53 [8.8%]	59 [9.9%]	61 [10.1%]
Generously allowed	2 [0.3%]	0 [0.0%]	4 [0.7%]
Disallowed	0 [0.0%]	2 [0.3%]	2 [0.3%]
R.m.s. deviations			
Bond lengths (Å)	0.002	0.006	0.002
Bond angles (°)	0.574	0.641	0.568
Dihedral angles (°)	10.9	11.8	13.7

† Data taken from Zhou *et al.* (2009) or from the corresponding PDB entry 2r7i and referring to space group $P4_3$. ‡ According to *PROCHECK* from the *CCP*4 suite (Winn *et al.*, 2011).

resolution structure of the same complex (PDB entry 3pe1; Battistutta *et al.*, 2011) originating from pre-incubation of the enzyme and the inhibitor prior to crystallization revealed no significant difference in the hinge/αD region from the original structure (Ferguson *et al.*, 2011).

After submission of this manuscript, three new human CK2α structures with the low-density tetragonal crystal packing were released (Papinutto *et al.*, 2012). They are not included in Table 1, but as discussed below they support the insights from this work.

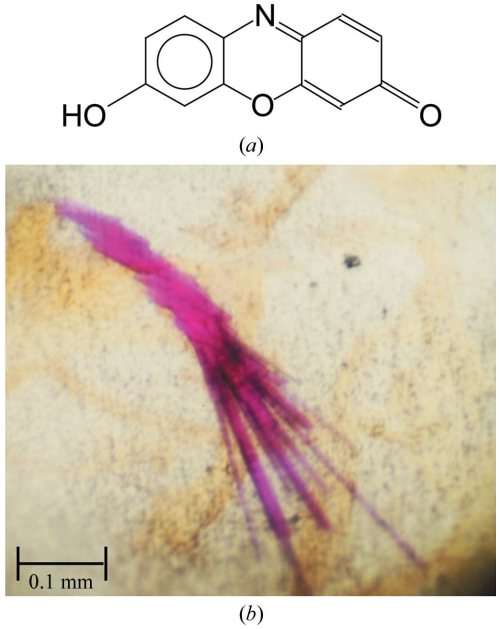

Figure 3
Cocrystallization of CK2α^{1-335} with resorufin. (*a*) Structure of resorufin. (*b*) CK2α^{1-335} crystals grown in the presence of resorufin.

2.2. Protein preparation and crystallization

Human CK2α^{1-335} was recombinantly expressed in *Escherichia coli* BL21 (DE3) cells and purified as described by Raaf, Klopffleisch *et al.* (2008). Finally, the CK2α^{1-335} solution was concentrated by ultrafiltration and rebuffered in 500 m*M* NaCl, 25 m*M* Tris–HCl pH 8.5. The final protein concentration was 10.0 mg ml^{-1}.

Resorufin was purchased from Sigma–Aldrich. A 10 m*M* resorufin solution was prepared in the same buffer but with the addition of 5% DMSO. Equal volumes of the CK2α^{1-335} solution and the resorufin stock solution were mixed, pre-incubated for 45 min at room temperature and used in vapour-diffusion crystallization experiments. CK2α^{1-335}–resorufin crystals (Fig. 3*b*) grew from drops consisting of equal volumes of CK2α^{1-335}–resorufin mixture and a reservoir solution composed of 30% PEG 8000, 0.2 *M* ammonium sulfate, 0.1 *M* sodium cacodylate pH 6.4. Details of the production and

crystallization of the CK2α^{1-325}/CK2$\alpha'^{327-350}$ construct in the presence of AMPPNP and magnesium ions have recently been described (Bischoff, Raaf *et al.*, 2011).

2.3. Diffraction data collection, structure determination and optimization

X-ray diffraction data were collected from cryocooled CK2α^{1-335}–resorufin crystals (cryosolution: 30% PEG 8000, 20% glycerol, 0.2 *M* ammonium sulfate, 0.1 *M* sodium cacodylate pH 6.4) at a temperature of 100 K on beamline 14.1 of the BESSY synchrotron, Berlin, Germany. The wavelength was 0.91841 Å. We used *XDS* (Kabsch, 2010) to integrate the diffraction data and *SCALA* (Evans, 2006) from the *CCP*4 suite (Winn *et al.*, 2011) to scale the data. We applied the same procedure to process a CK2α^{1-325}/CK2$\alpha'^{327-350}$ diffraction data set that had been collected in the context of the published structure 3rp0 (Bischoff, Raaf *et al.*, 2011). These diffraction data were different from the raw data underlying structure 3rp0 (Bischoff, Raaf *et al.*, 2011), but the two corresponding crystals had been grown under equivalent conditions.

The *XDS* integration runs were performed without symmetry specification (*i.e.* in space group *P*1) and ran stably without lattice constraints. After integration the space group was automatically determined to be $P4_12_12$ (or its enantiomorph $P4_32_12$) by the *XDS* routine *CORRECT* (Kabsch, 2010) in both cases and this assignment was confirmed by *POINTLESS* (Evans, 2006) from the *CCP*4 suite (Winn *et al.*, 2011).

The high-resolution limits of the CK2α^{1-335}–resorufin and CK2α^{1-325}/CK2$\alpha'^{327-350}$ diffraction data sets were determined by visual inspection of single images and on the basis of the $\langle I/\sigma(I)\rangle$ ratios in the last shells (Table 2). A possible reason for the relatively high $R_{\rm merge}$ values of the data sets (in particular in the case of the CK2α^{1-335}–resorufin complex) is an increased portion of weak reflections caused by pseudo-centring, as documented in Fig. 4. However, the $R_{\rm merge}$ value in the top intensity bin was lower than 4%, indicating the absence of systematic errors.

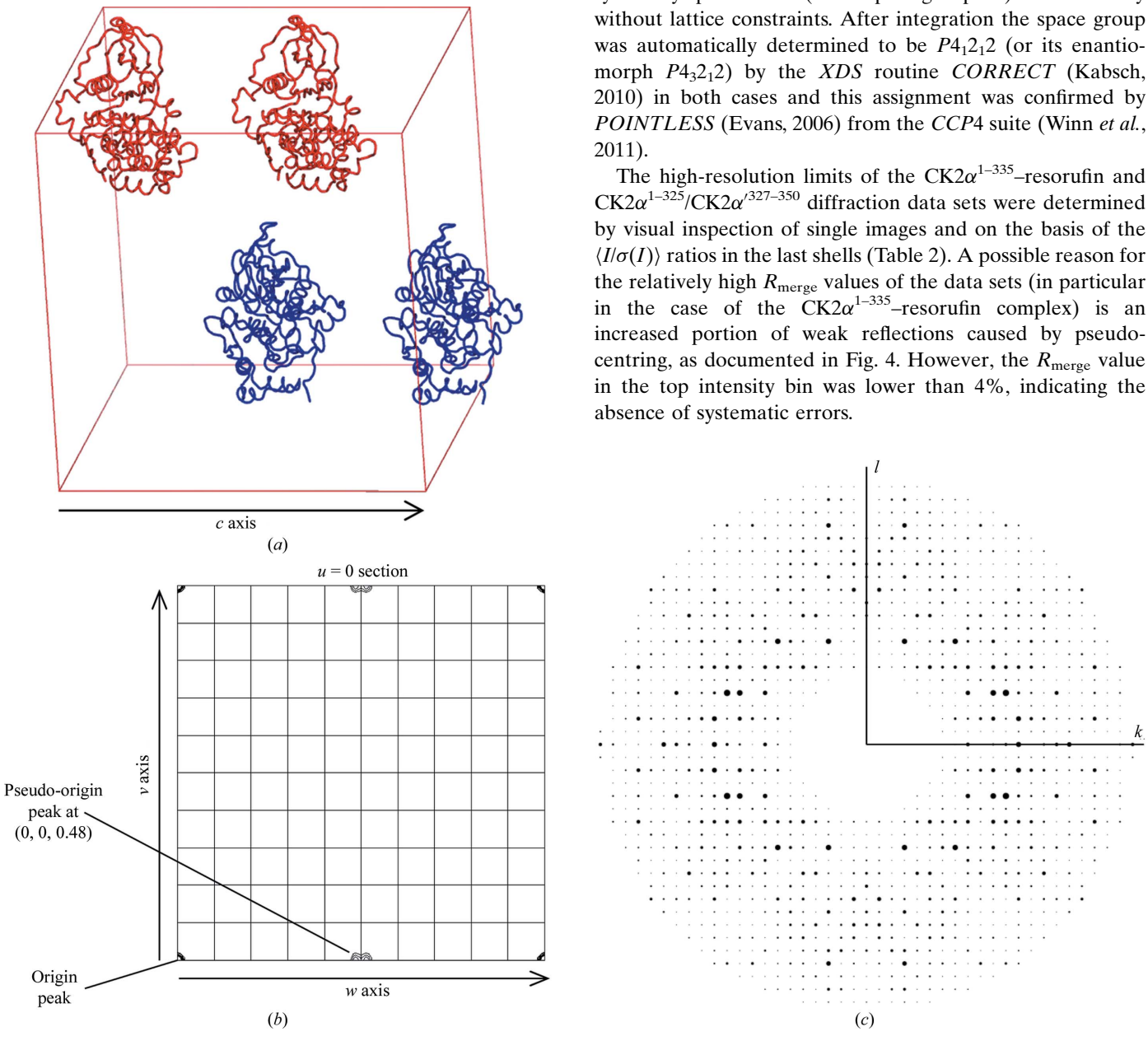

Figure 4
Pseudo-centring of the low-density tetragonal crystal form and its consequences for X-ray diffraction. (*a*) Crystallographic unit cell with two pairs of CK2α molecules. The two members of each pair are related by the translation vector (0, 0, 0.48). (*b*) $u = 0$ section of a native Patterson function. The Patterson density was drawn with a cutoff of 20σ (statistics over the whole unit cell). (*c*) Consequences of the pseudo-centring in the crystal packing for X-ray diffraction illustrated by the (0*kl*) section of the CK2α^{1-335}–resorufin diffraction data set with a high-resolution cutoff at 6 Å. Odd *l* indices lead to a systematic weakening of X-ray reflections in the region of small *l* indices. The figure was prepared with the reflection-data viewer in *PHENIX* (Adams *et al.*, 2010). All parts of the figure were prepared using data for the CK2α^{1-335}–resorufin structure.

Finally, as a third data set, the apo CK2α^{1-335} structure factors (PDB entry 2r7i; Zhou *et al.*, 2009) were downloaded from the PDB. In this case *POINTLESS* (Evans, 2006) also assigned $P4_12_12$ or its enantiomorph $P4_32_12$ as the correct space group, but owing to the lack of raw diffraction data no full re-processing was performed.

The subsequent procedure was equivalent in all three cases. The CK2α^{1-335}–CX-4945 structure (PDB entry 3nga; Ferguson *et al.*, 2011), with all atomic coordinates corresponding to water, ligands and hinge/αD residues removed, served as a starting point for refinement performed by *PHENIX* (Adams *et al.*, 2010) supported by manual optimization with *Coot* (Emsley *et al.*, 2010). Automatically assigned torsion-angle NCS restraints were applied in *phenix.refine* runs. Optimal weighting factors between X-ray and stereochemistry terms were determined automatically by *PHENIX*.

2.4. Molecular-replacement and refinement test calculations

To rationalize previous molecular-replacement and refinement problems with PDB entries 2r7i (Zhou *et al.*, 2009) and 3rp0 (Bischoff, Raaf *et al.*, 2011), we performed retrospective molecular-replacement and refinement test calculations using *MOLREP* (Vagin & Teplyakov, 2010), *Phaser* (McCoy *et al.*, 2007) and *REFMAC* (Murshudov *et al.*, 2011) in the versions embedded in release 6.2.0 of the *CCP*4 suite (Winn *et al.*, 2011).

2.5. Calculation of differential solvent accessibilities

The solvent-accessible surface areas of CK2α chains covered by symmetry equivalents (Table 1, column 6) were calculated using *AREAIMOL* from the *CCP*4 suite (Winn *et al.*, 2011). All nonprotein atoms were neglected in these calculations.

3. Results and discussion

3.1. Structural optimization

PDB entries 2r7i and 3rp0, which are two of the structures with the low-density tetragonal packing No. 5 in Table 1, were published with the lower symmetrical space group $P4_3$ rather than $P4_32_12$ (Zhou *et al.*, 2009; Bischoff, Raaf *et al.*, 2011). In the case of 3rp0 from our group, data processing and molecular-replacement searches with *Phaser* (McCoy *et al.*, 2007) from the *CCP*4 package (Winn *et al.*, 2011) initially indicated $P4_32_12$ as the correct space group, but subsequent refinement runs with *REFMAC* stuck at $R_{\rm free}$ values of around 40%. Convergence could only be achieved by reducing the symmetry to space group $P4_3$, but at the expense of more model bias. The authors of structure 2r7i (Zhou *et al.*, 2009) encountered similar problems and likewise reduced the symmetry in order to overcome them (Y. Shen, personal communication).

Subsequently, the publication of the isomorphous structure 3nga (Ferguson *et al.*, 2011) indicated that refinement in space group $P4_32_12$, and thus with a reduced asymmetric unit containing two rather than four independent subunits, should be possible. This was confirmed here by taking the ligand-free 3nga coordinates as a starting point for refinement, which was successful (Table 2).

$P4_32_12$-based refinement resulted in structures of significantly better quality. For instance, in all four CK2α^{1-335} chains of the original PDB entry 2r7i (Zhou *et al.*, 2009) several residues of the ATP-binding loop and the $\beta4\beta5$ loop (Fig. 1) were omitted owing to disorder; after the novel refinement the $\beta4\beta5$ loops of both chains and one of the ATP-binding loops were well defined. A glycerol molecule from the cryosolution was visible at the ATP site (Fig. 2*c*).

In the case of the CK2α^{1-325}/CK2$\alpha'^{327-350}$ structure (Bischoff, Raaf *et al.*, 2011) the optimization depended on the processing of better raw data (see above) combined with assignment of the higher symmetrical space group. Here, clear electron density indicated the presence of the nucleotide analogue in the ATP-binding site (Fig. 2*a*), yet in the region of the imido-triphospho moiety the picture was not unambiguous. In a similar case (PDB entry 3nsz), Ferguson *et al.* (2011) assumed hydrolysis under the acidic pH conditions of the crystallization drop, deleted the terminal phosphono moiety of AMPPNP and referred to the remaining hydrolysis product adenylyl phosphoamidate as 'AMPPN'. We followed this practice partly and placed AMPPN into one chain and AMPPNP into the other accompanied by two Mg^{2+} ions.

3.2. Retrospective test calculations

In order to understand the previous convergence problems for PDB entries 2r7i and 3rp0, we compared the methods sections of the corresponding publications and found that, in contrast to Zhou *et al.* (2009) and Bischoff, Raaf *et al.* (2011), Ferguson *et al.* (2011) had used *MOLREP* (Vagin & Teplyakov, 2010) rather than *Phaser* (McCoy *et al.*, 2007) for molecular-replacement calculations. Therefore, we performed test calculations with the three $P4_32_12$-scaled data sets in Table 2 plus the structure factors belonging to PDB entry 3nga using the *CCP*4-integrated versions of *Phaser* and *MOLREP* followed by refinement with *REFMAC* (Murshudov *et al.*, 2011). In all cases *MOLREP* led to refinable solutions, while the *Phaser* solutions were not completely wrong (consistent with $R_{\rm free}$ values of around 40%) but were too inaccurate for subsequent convergence in refinement.

A possible explanation for this difference is that the crystallographic unit cell contains eight pairs of CK2α chains of approximately the same orientation related by the translation vector (0, 0, 0.48) (Fig. 4*a*). This special arrangement leads to a pseudo-origin peak in a native Patterson function (Fig. 4*b*) and to systematic weakening of X-ray reflections with an odd l index (Fig. 4*c*). Unlike *Phaser*, *MOLREP* automatically detects and exploits such translation vectors.

3.3. Complex structure of human CK2α^{1-335} with resorufin

The cocrystallization of resorufin and CK2α^{1-335} led to crystals with a significantly violet colour (Fig. 3*b*). The electron density at the ATP-binding site documents the binding of resorufin (Fig. 2*b*). However, it does not cover the ligand

completely, which led to high temperature factors and occupancies significantly below 1. This reflects a relatively low affinity, which is consistent with the micromolar K_i value (1.3 μ*M*) reported by Sandholt *et al.* (2009).

The low resolution of 3.2 Å and the limited quality of the electron-density map around the ligand only allow a preliminary view of the details of resorufin binding. At such a resolution water molecules often cannot be identified unambiguously. Nevertheless, it appears that resorufin penetrates relatively deeply into a region of the ATP-binding site that is typically blocked by a conserved water molecule (Battistutta *et al.*, 2007; Fig. 2*b*). Harboured in a well characterized hydrophobic pocket (Yde *et al.*, 2005; Battistutta, 2009) and flanked by nonpolar residues on both sides (Ile174 and Met163 on the C-terminal domain side and Val66 and Phe113 on the opposite side), resorufin binding requires no clearly defined hydrogen bonds to the enzyme matrix, in particular not to the hinge/αD region.

A curious feature of the crystal packing of the CK2α–resorufin complex that was not found in any other human or maize CK2α crystal form is an 'arginine zipper', *i.e.* a set of six alternating arginine side chains from two symmetry-equivalent enzyme subunits (Fig. 5*a*). A similar yet less well formed arginine-zipper motif is present in the second low-density crystal form of Table 1 corresponding to the CK2 holoenzyme (Fig. 5*b*; Niefind *et al.*, 2001). A recent analysis has shown that this 'electrostatics-defying interaction between arginine termini' (Pednekar *et al.*, 2009) occurs surprisingly frequently and is even a driving force of protein–protein interactions. To our knowledge, however, such an extended motif as the arginine zipper in Fig. 5 has not been described before.

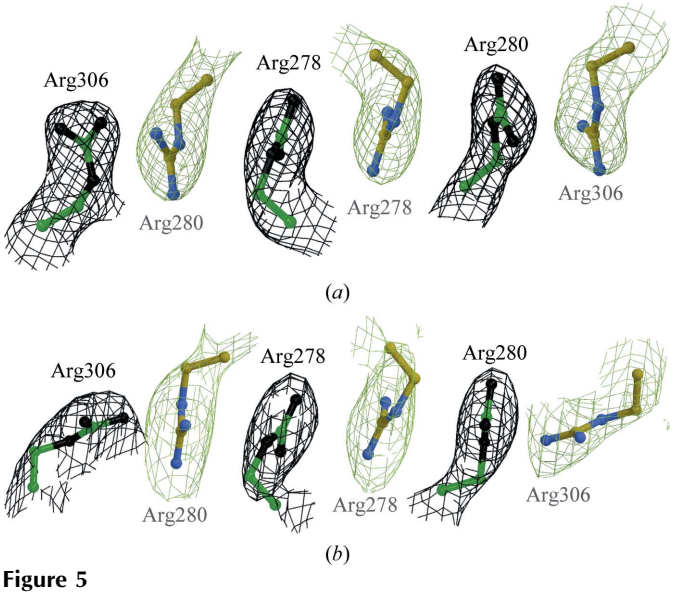

Figure 5
An 'arginine zipper' mediating a protein–protein interaction at a crystal contact. The guanidinium moieties of six arginine side chains are arranged in a helical manner and are provided alternately by each of the two protein subunits. The positive charges are balanced by neighbouring negatively charged side chains and ions (not drawn). The pieces of electron density were drawn with a 1σ cutoff level. The figure was prepared with *BobScript* (Esnouf, 1997) and *Raster3D* (Merritt & Bacon, 1997). (*a*) Arginine zipper in the low-density tetragonal crystal form represented by the CK2α^{1-335}–resorufin structure. (*b*) Distorted arginine zipper in the low-density hexagonal crystal form of the CK2 holoenzyme (PDB entry 1jwh; Niefind *et al.*, 2001).

3.4. Hinge/αD-region preferences

The hinge/αD region of each chain of the CK2α^{1-335}–resorufin structure is found in the closed conformation (Fig. 2*b*). Assignment to either the open or the closed conformation can be easily performed for any CK2α structure, since an unambiguous flag exists in Phe121 (Bischoff, Raaf *et al.*, 2011; Battistutta & Lolli, 2011). Phe121 is topologically equivalent to the catalytic spine member Met128 of CAPK, and like the latter it can bury its side chain in a hydrophobic cavity and thus complete the catalytic spine. This 'Phe121-in' state (Fig. 1), as observed in the CK2α^{1-335}–resorufin complex (Fig. 2*b*), is equivalent to the closed hinge/αD region conformation, which is thus 'canonical' with respect to CAPK and other EPKs (Bischoff, Raaf *et al.*, 2011; Battistutta & Lolli, 2011). It is atypical, however, with respect to maize CK2α, to the CK2 holoenzyme and to the paralogous isoform human CK2α′ (Bischoff, Olsen *et al.*, 2011), all of which display an open hinge/αD region with Phe121 turned to an 'out' state (Fig. 1). In this state the aromatic side chain fills a space that is otherwise occupied by Lys122 (Battistutta & Lolli, 2011).

Similar to the CK2α^{1-335}–resorufin complex, the hinge/αD region adopts a closed conformation in apo CK2α^{1-335} (Fig. 2*c*), while it is fixed in the open conformation in both subunits of the complex with the inhibitor CX-4945 (Ferguson *et al.*, 2011; the black reference in Fig. 2 representing the open conformation) and of the CK2α^{1-325}/CK2$\alpha'^{327-350}$–AMPPN(P) complex (Fig. 2*a*). The statistical basis of this equipartition, with four chains open and four chains closed, is thin, but nevertheless it permits the preliminary conclusion that this low-density crystal packing does not *per se* prefer either of the two conformational states over the other.

This notion is supported by the fact that the crystal contacts of the hinge/αD regions are small in this packing (No. 5 in Table 1) and, in contrast to the monoclinic crystal form, do not differ significantly between the open and the closed hinge/αD conformations. It was further confirmed by three CK2α structures recently published by Papinutto *et al.* (2012) that likewise belong to packing No. 5 in Table 1: in these structures one of the two CK2α chains of the asymmetric unit adopts an open hinge/αD region conformation and the other adopts a closed conformation.

Notably, the electron densities and temperature factors of the hinge/αD regions reveal the following tendencies: (i) in each of the eight chains the hinge/αD region is among the zones with the largest internal disorder and (ii) the degree of disorder in the hinge/αD region is significantly higher in the chains with closed conformation. These findings suggest that there is not only conformational ambiguity in the hinge/αD region of human CK2α but rather a dynamic conformational equilibrium in solution that can be resolved by suitable ligands

favouring one of the two conformations either by stabilizing it or by destabilizing the other conformation.

The CK2α^{1-325}/CK2$\alpha'^{327-350}$–AMPPN(P) complex (Fig. 2*a*) suggests that the physiological cosubstrate ATP that normally causes the final closure of the catalytic spine (Kornev *et al.*, 2008; Taylor & Kornev, 2011; Fig. 1) in this case supports the open hinge/αD conformation with an incomplete catalytic spine. However, it is unclear how this is achieved since the only interactions of AMPPN(P) with the hinge/αD region are hydrogen bonds to Glu114 and Val116 (Fig. 2*a*), *i.e.* to the N-terminal part of the hinge/αD region, in which the two conformations are not yet different.

3.5. Which factors are responsible for the hinge/αD-region conformation of CK2α?

In all of its crystal structures (more than 30) maize CK2α exists with an open hinge/αD conformation, irrespective of the ligand, the crystallization conditions or the crystal packing. Thus, in maize CK2α strong intramolecular constraints must exist that enforce an unambiguous local conformation (in addition to that atypical for EPKs; Bischoff, Raaf *et al.*, 2011; Battistutta & Lolli, 2011). Initial plausible ideas about the critical amino acids that cause this conformational discrimination have recently been suggested (Battistutta & Lolli, 2011).

In human CK2α, however, the intrinsic constraints are significantly weaker, so that external factors such as ligand binding, temperature, ionic strength, pH value and crystal packing come into play. We previously assumed (Niefind & Issinger, 2010) that CK2β, although not binding directly to the hinge/αD region, might shift the conformational equilibrium towards the open state, but owing to the lack of more than one structure (PDB entry 1jwh; Niefind *et al.*, 2001) this remains an unproven hypothesis.

One clear tendency, however, is visible from an inspection of Table 1, namely that high concentrations of lyotropic salts enforce the closed conformation: in all structures of packing 4a in Table 1 and the very similar packing 4b the hinge/αD region is closed and typically relatively well ordered. These structures originate from high-density tetragonal crystal packings in which the hinge/αD region is not involved in (and thus is not affected by) crystal contacts. Modelling of the open hinge/αD state into these structures with *Coot* (Emsley *et al.*, 2010) revealed that it would likewise be compatible with these crystal packings.

A common and distinctive feature of these structures is that the corresponding crystallization media are free of polyethylene glycol and are dominated by high concentrations of salts with lyotropic anions (citrate, sulfate and chloride). As known from the 'salting-out' effect of proteins and from hydrophobic interaction chromatography, such anions support hydrophobic interactions (Queiroz *et al.*, 2001) by interacting with water, lowering its surface tension and disturbing the water shell around hydrophobic surfaces.

With regard to human CK2α, this means that the closed hinge/αD conformation is strongly supported by lyotropic salts because (i) only in this conformation can Phe121 harbour its aromatic side chain in the hydrophobic C-spine environment and (ii) water molecules that stabilize the open hinge/αD conformation by occupation of a cavity near Asn118 between the hinge and the rest of the enzyme (Fig. 2*a*) are removed, as noted previously by Battistutta & Lolli (2011). It will be interesting to investigate in the future whether chaotropic anions such as nitrate or thiocyanate have the opposite effect and favour the open hinge/αD conformation.

The dominance of this 'high lyotropic salt effect' is relevant to the open question of which of the two hinge/αD conformations of human CK2α is the active one. In previous studies (Bischoff, Raaf *et al.*, 2011; Niefind & Issinger, 2010) we favoured the open state because of the equivalence to maize CK2α and owing to the observation that binding of an ATP analogue is correlated in most cases with an open hinge/αC region (PDB entries 1pjk, 2pvr, 3nsz, 3u87 and 1jwh; Table 1). Recently, however, the only exception (PDB entry 3juh; Yde *et al.*, 2005) was taken as an argument that human CK2α might also be active with a closed hinge/αC region (Battistutta & Lolli, 2011), but the study presented here suggests that the exceptional combination of AMPPNP binding and closed hinge/αD conformation is a consequence of the dominating high citrate concentration and does not represent a functional state. This conclusion is also consistent with the early observation that increasing chloride concentrations strongly reduce the catalytic activity of human CK2α (Grankowski *et al.*, 1991).

In any case, the example of 3juh demonstrates that genuine effects of ATP-site ligands on the hinge/αD conformation can best be observed under moderate salt concentrations with variants of (poly)ethylene glycol as precipitant. Fortunately, under such conditions apo CK2α itself does not show a clear conformational preference: as the apo structures 1na7 and 2r7i demonstrate, subtle effects [such as possibly the pH value or the nature of the salt additive (the strongly lyotropic sulfate in 2r7i *versus* the weakly lyotropic acetate in 1na7)] can determine whether the hinge/αD region is open (1na7) or closed (2r7i), again illustrating the small size of the energetic difference between the two states.

As indicated in §1, crystal-packing constraints may cause a certain bias in the monoclinic crystal form (No. 1 in Table 1) but they do not dominate. This was impressively shown by López-Ramos *et al.* (2010) by the comparison of structures 3mb6 and 3mb7. In both cases the corresponding monoclinic CK2α^{1-335} crystals originally grew under conditions that were known to support the open hinge/αD conformation (Ermakova *et al.*, 2003), but extensive soaking (one week) with the respective ATP-competitive inhibitors enforced the closed hinge/αD conformation in one case, while in the other the open conformation was retained. Neither of these two inhibitors forms hydrogen bonds similar to the adenine moiety of ATP, *i.e.* to Glu114 and Val116 in the N-terminal part of the hinge/αD region (Fig. 2*a*). Rather, López-Ramos *et al.* (2010) identified Asn118 as a critical residue: in structure 3mb7 (but not in 3mb6) the Asn118 side chain forms a hydrogen bond to the corresponding inhibitor and requires

the hinge/αD region in its open conformation for this interaction.

An equivalent hydrogen bond is not present if the open hinge/αD conformation is combined with AMPPNP or with the inhibitor CX-4945 (Fig. 2*a*). Thus, while no general rule is apparent so far, in the case of particular ligands single enzyme–ligand hydrogen bonds may be critical for the decision between the open and the closed hinge/αD conformation, suggesting that virtual screening efforts should always include both hinge/αD conformations.

For further experimental investigations of the conformational plasticity of human CK2α, it is noteworthy that the closed hinge/αD conformation in structure 3mb6 (as opposed to 3mb7) suffers from a high degree of disorder, which may indicate a considerable bias that enters into play when the soaking technique is applied in a case in which crystal-packing constraints are not eliminated. Therefore, the low-density tetragonal crystals of the CK2α–resorufin complex investigated in this work provide a more suitable crystalline basis for the study of such ligand-imposed conformational switches of the hinge/αD region in human CK2α.

4. Accession codes

The final atomic coordinates and structure-factor amplitudes of the CK2α^{1-335}–resorufin complex are available from the PDB (accession code 3u9c). The improved structure of the CK2α^{1-325}/CK2$\alpha'^{327-350}$–AMPPN(P) complex was deposited in the PDB under accession code 3u87, which replaces entry 3rp0.

We are grateful to the staff of the BESSY synchrotron, Berlin, Germany for assistance with data collection and to Elena Brunstein for excellent technical assistance in protein purification and crystallization. The valuable comments of Professor Yuequan Shen, Nankai University, Tianjin, People's Republic of China on the refinement problems with structure 2r7i are gratefully acknowledged. This work was funded by the Danish Research Council (grant No. 21-01-0511) and by the Deutsche Forschungsgemeinschaft (DFG; grant NI 643/4-1).

References

Adams, P. D. *et al.* (2010). *Acta Cryst.* D**66**, 213–221.
Battistutta, R. (2009). *Cell. Mol. Life Sci.* **66**, 1868–1889.
Battistutta, R., Cozza, G., Pierre, F., Papinutto, E., Lolli, G., Sarno, S., O'Brien, S. E., Siddiqui-Jain, A., Haddach, M., Anderes, K., Ryckman, D. M., Meggio, F. & Pinna, L. A. (2011). *Biochemistry*, **50**, 8478–8488.
Battistutta, R. & Lolli, G. (2011). *Mol. Cell. Biochem.* **356**, 67–73.
Battistutta, R., Mazzorana, M., Cendron, L., Bortolato, A., Sarno, S., Kazimierczuk, Z., Zanotti, G., Moro, S. & Pinna, L. A. (2007). *Chembiochem*, **8**, 1804–1809.
Bischoff, N., Olsen, B., Raaf, J., Bretner, M., Issinger, O.-G. & Niefind, K. (2011). *J. Mol. Biol.* **407**, 1–12.
Bischoff, N., Raaf, J., Olsen, B., Bretner, M., Issinger, O.-G. & Niefind, K. (2011). *Mol. Cell. Biochem.* **356**, 57–65.
Cox, S., Radzio-Andzelm, E. & Taylor, S. S. (1994). *Curr. Opin. Struct. Biol.* **4**, 893–901.
Emsley, P., Lohkamp, B., Scott, W. G. & Cowtan, K. (2010). *Acta Cryst.* D**66**, 486–501.
Ermakova, I., Boldyreff, B., Issinger, O.-G. & Niefind, K. (2003). *J. Mol. Biol.* **330**, 925–934.
Esnouf, R. M. (1997). *J. Mol. Graph.* **15**, 132–134.
Evans, P. (2006). *Acta Cryst.* D**62**, 72–82.
Ferguson, A. D., Sheth, P. R., Basso, A. D., Paliwal, S., Gray, K., Fischmann, T. O. & Le, H. V. (2011). *FEBS Lett.* **585**, 104–110.
Fritz, G., Issinger, O.-G. & Olsen, B. B. (2009). *Int. J. Oncol.* **35**, 1151–1157.
Grankowski, N., Boldyreff, B. & Issinger, O.-G. (1991). *Eur. J. Biochem.* **198**, 25–30.
Guerra, B. & Issinger, O.-G. (2008). *Curr. Med. Chem.* **15**, 1870–1886.
Kabsch, W. (2010). *Acta Cryst.* D**66**, 125–132.
Knighton, D. R., Zheng, J.-H., Ten Eyck, L. F., Ashford, V. A., Xuong, N.-H., Taylor, S. S. & Sowadski, J. M. (1991). *Science*, **253**, 407–414.
Kornev, A. P., Taylor, S. S. & Ten Eyck, L. F. (2008). *Proc. Natl Acad. Sci. USA*, **105**, 14377–14382.
López-Ramos, M., Prudent, R., Moucadel, V., Sautel, C. F., Barette, C., Lafanechère, L., Mouawad, L., Grierson, D., Schmidt, F., Florent, J. C., Filippakopoulos, P., Bullock, A. N., Knapp, S., Reiser, J. B. & Cochet, C. (2010). *FASEB J.* **24**, 3171–3185.
McCoy, A. J., Grosse-Kunstleve, R. W., Adams, P. D., Winn, M. D., Storoni, L. C. & Read, R. J. (2007). *J. Appl. Cryst.* **40**, 658–674.
Merritt, E. A. & Bacon, D. J. (1997). *Methods Enzymol.* **277**, 505–524.
Murshudov, G. N., Skubák, P., Lebedev, A. A., Pannu, N. S., Steiner, R. A., Nicholls, R. A., Winn, M. D., Long, F. & Vagin, A. A. (2011). *Acta Cryst.* D**67**, 355–367.
Niefind, K., Guerra, B., Ermakowa, I. & Issinger, O.-G. (2001). *EMBO J.* **20**, 5320–5331.
Niefind, K., Guerra, B., Pinna, L. A., Issinger, O.-G. & Schomburg, D. (1998). *EMBO J.* **17**, 2451–2462.
Niefind, K. & Issinger, O.-G. (2010). *Biochim. Biophys. Acta*, **1804**, 484–492.
Niefind, K., Raaf, J. & Issinger, O.-G. (2009). *Cell. Mol. Life Sci.* **66**, 1800–1816.
Papinutto, E., Ranchio, A., Lolli, G., Pinna, L. A. & Battistutta, R. (2012). *J. Struct. Biol.* **177**, 382–391.
Pechkova, E., Zanotti, G. & Nicolini, C. (2003). *Acta Cryst.* D**59**, 2133–2139.
Pednekar, D., Tendulkar, A. & Durani, S. (2009). *Proteins*, **74**, 155–163.
Queiroz, J. A., Tomaz, C. T. & Cabral, J. M. S. (2001). *J. Biotechnol.* **87**, 143–159.
Raaf, J., Brunstein, E., Issinger, O.-G. & Niefind, K. (2008). *Chem. Biol.* **15**, 111–117.
Raaf, J., Issinger, O.-G. & Niefind, K. (2009). *J. Mol. Biol.* **386**, 1212–1221.
Raaf, J., Klopffleisch, K., Issinger, O.-G. & Niefind, K. (2008). *J. Mol. Biol.* **377**, 1–8.
Sandholt, I. S., Olsen, B. B., Guerra, B. & Issinger, O.-G. (2009). *Anticancer Drugs*, **20**, 238–248.
Siddiqui-Jain, A., Drygin, D., Streiner, N., Chua, P., Pierre, F., O'Brien, S. E., Bliesath, J., Omori, M., Huser, N., Ho, C., Proffitt, C., Schwaebe, M. K., Ryckman, D. M., Rice, W. G. & Anderes, K. (2010). *Cancer Res.* **70**, 10288–10298.
Taylor, S. S. & Kornev, A. P. (2011). *Trends Biochem. Sci.* **36**, 65–77.
Traxler, P. & Furet, P. (1999). *Pharmacol. Ther.* **82**, 195–206.
Trembley, J. H., Chen, Z., Unger, G., Slaton, J., Kren, B. T., Van Waes, C. & Ahmed, K. (2010). *Biofactors*, **36**, 187–195.
Vagin, A. & Teplyakov, A. (2010). *Acta Cryst.* D**66**, 22–25.
Winn, M. D. *et al.* (2011). *Acta Cryst.* D**67**, 235–242.
Yde, C. W., Ermakova, I., Issinger, O.-G. & Niefind, K. (2005). *J. Mol. Biol.* **347**, 399–414.
Zheng, J., Knighton, D. R., Ten Eyck, L. F., Karlsson, R., Xuong, N., Taylor, S. S. & Sowadski, J. M. (1993). *Biochemistry*, **32**, 2154–2161.
Zhou, W. H., Qin, X. H., Yan, X. J., Xie, X. Q., Li, L., Fang, S. S., Long, J. F., Adelman, J., Tang, W.-J. & Shen, Y. Q. (2009). *Chin. Sci. Bull.* **54**, 220–226.